Pathways and modification of the upper and intermediate waters of the Arctic Ocean

Michael J. Karcher

Alfred Wegener Institute for Polar and Marine Research, Bremerhaven, Germany

Josef M. Oberhuber[1]

German Climate Computing Centre (DKRZ), Hamburg, Germany

[1] The purpose of this study is to investigate the pathways and the ventilation of source water masses of the upper and intermediate waters of the Arctic Ocean. For the Arctic and subarctic domain a coupled ice-ocean general circulation model is set up to be integrated for several decades. It is driven by a climatological seasonal cycle of monthly mean atmospheric data from 1980 to 1989 and by restored sea surface salinities. Passive tracers are used to visualize and interpret the modeled flow and to compare it with observations. The model is able to reproduce known features of the Arctic Ocean circulation like the inflow of two branches of Atlantic origin via the Fram Strait and the Barents Sea and their subsequent passage at middepths in several cyclonic circulation cells. The fate of these Atlantic source water masses, river water, and Bering Strait inflow water in the model are studied. The branch crossing the Barents Sea is subject to an intense heat loss and ice formation. As a result, water of this branch leaves the shelf toward the central part of the Arctic Ocean not only at the surface but also in denser varieties, which finally feed the central Arctic at halocline and middepths. The lightest part turns northward and finally westward joining the Transpolar Drift; the densest part (200–1000 m depth) moves eastward along the continental slope. A similar path is taken by the Atlantic water branch from the Fram Strait. The inflowing branch over the Barents Sea turns out to be the dominant source for the lower Atlantic Water layer in the Arctic Ocean in this investigation. Atlantic tracers starting in Fram Strait need 6 years to reach the northern Laptev Sea slope. Travel times to return to Fram Strait are 15–20 years along the Lomonossov Ridge and about 30 years along the continental slope of the Canadian Basin. Tracers that mark the Pacific Water or the Mackenzie River Water flow eastward and leave the Arctic mainly via the Canadian Archipelago. The Siberian River water tracers at the surface penetrate far into the Canadian Basin before they join the Transpolar Drift. The travel times of the river water from the river mouths are 2–3 years to the shelf edge and 12–14 years to Fram Strait. *INDEX TERMS:* 4207 Oceanography: General: Arctic and Antarctic oceanography; 4255 Oceanography: General: Numerical modeling; 4536 Oceanography: Physical: Hydrography; 4572 Oceanography: Physical: Upper ocean processes; *KEYWORDS:* Arctic Ocean, Atlantic Water layer, Barents Sea Water, Halocline, dense water formation, layer model

1. Introduction

[2] Under a cover of ice and snow the central part of the Arctic Ocean is strongly stratified. A fresh and cold surface layer, several tens of meters thick, is separated by a strong halocline from warm and salty water of Atlantic origin in 200–1000 m depth. The movement of the ice and the flow at the ocean's surface are assumed to follow similar pathways: the Transpolar Drift (TPD) runs from the Siberian Shelves toward Fram Strait, while the Beaufort Gyre, a large anticyclonic flow, occupies parts of the Canadian Basin and feeds the TPD. Since the Arctic Ocean is one of the source regions for deep and intermediate waters of the Northern Hemisphere [*Anderson et al.*, 1999; *Mauritzen*, 1996], the ventilation of its interior is important beyond its geographical borders. Because of the ice cover, the central part of the Arctic Ocean is largely prevented from local contact with the atmosphere; ventilation is provided by lateral exchange through the straits and with the shelf areas.

[3] Low-salinity Pacific Water enters through Bering Strait, and freshwater is added via the Siberian and Canadian Shelves by rivers and by the Norwegian Coastal Current moving into the Barents Sea. The sources for warm and salty water of Atlantic origin are the Fram Strait and the Barents Sea. The Atlantic Water that enters the Barents Sea between Spitsbergen and Norway is subject to a massive heat loss to the atmosphere [e.g., *Häkkinen and Cavalieri*, 1989] and to a blending with freshwater from melting, river runoff, and the Norwegian Coastal Current. In winter, salt is injected because of freezing. These processes lead to the formation of several varieties of water, which subsequently leave the Barents Sea toward the central Arctic Ocean or the adjacent Kara and Laptev Seas. The Barents Sea Branch Water (BSBW), the densest water on the eastern part of the shelf, enters the Eurasian Basin through the St. Anna Trough and sinks. On this way it encounters Fram Strait Branch Water (FSBW), an Atlantic Water branch that has entered through Fram Strait. A less dense variety of shelf water is formed in the

---

[1]Now at Am Loisachbogen 5a, Wolfratshausen, Germany.

B.S.: Bering Strait
C.P.: Chukchi Plateau
E.B.: Eurasian Basin
F.J.L.: Franz Josef Land
G.S.: Greenland Sea
C.B.: Canadian Basin
M.B.: Makarov Basin
Nov.S.: Nowaya Semlya
N.S.: Norwegian Sea
St.A.T.: St. Anna Trough
Sv.S.: Svernaya Semlya
Spitsb.: Spitsbergen
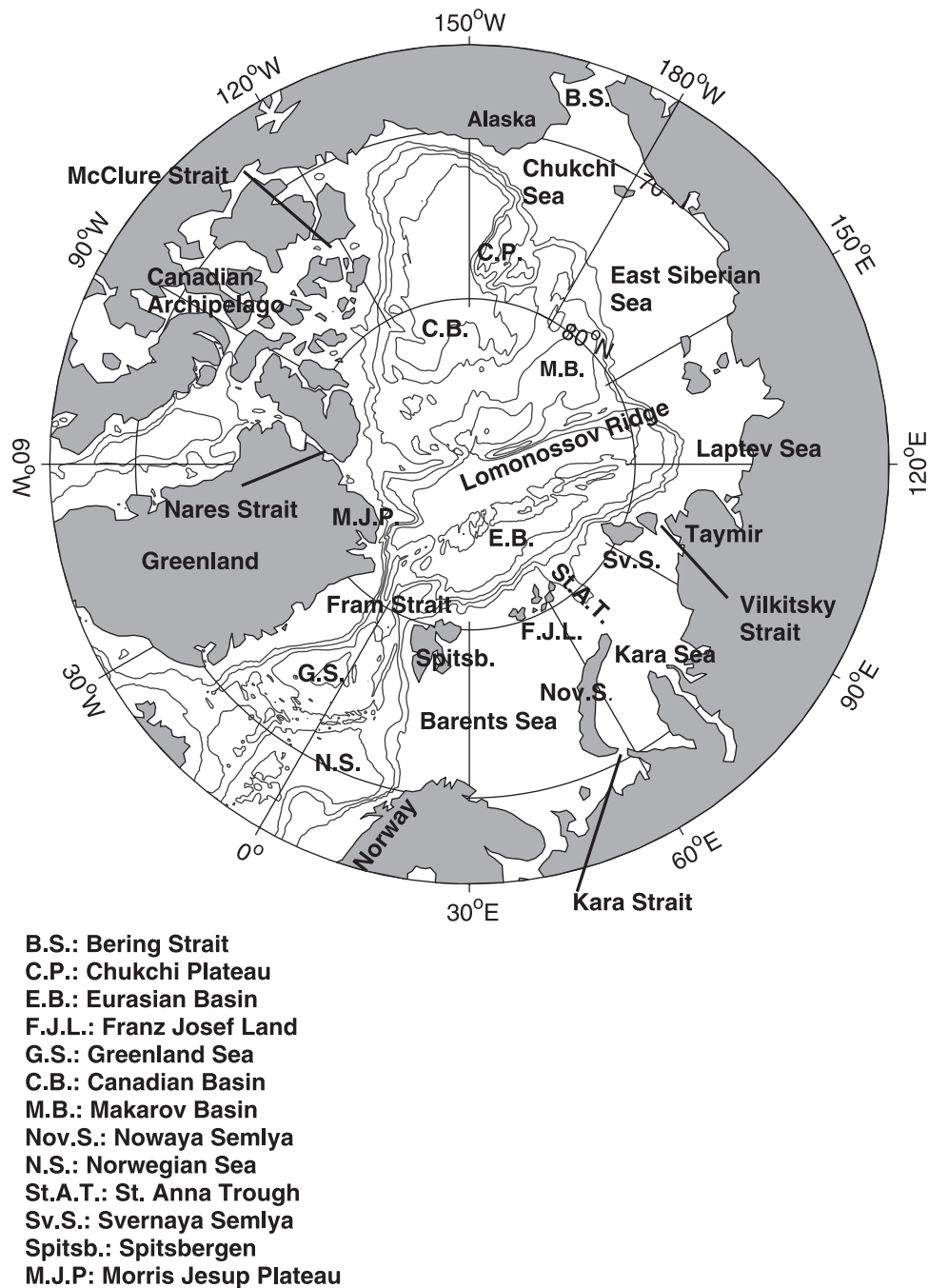M.J.P: Morris Jesup Plateau

Figure 1. (a) Geographical names used in the text. (b) The model topography given in meters. The thin solid line depicts the realistic coastline, while the shaded boxes show the land mask of the model. The thick shaded line shows the location of hydrographic sections referred to in the text. The numbered thick solid lines depict the locations of sections referred to in the text and in Table 1b.

northern Kara Sea by mixing with low-salinity water and is expected to flow northward and to the central Arctic Ocean [*Harms and Karcher*, 1999].

[4] It has been a common assumption that the major part of the lower halocline water is produced on the Barents Sea Shelf [*Aagaard et al.*, 1981]. More recent investigations from *Rudels et al.* [1996], however, point to the cycle of ice melt and freeze in the western Eurasian Basin as a second source. Here the halocline is in direct contact with the atmosphere. Ventilation pathways and timescales of the Arctic Ocean layers have been a focus in the interpretation of observed hydrographic and tracer data [e.g.,

Rudels et al., 1996; *Schlosser et al.*, 1995; *Bauch et al.*, 1995]; little attention, however, has been paid to them in numerical studies of the Arctic Ocean so far.

[5] In the present investigation we will analyze the seasonal cycle of the oceanic regime with respect to the replacement and ventilation of the upper and intermediate depth water with a coupled ice-ocean model. The model domain covers the Arctic Ocean, the Nordic Seas, and the Northern North Atlantic (Figures 1a and 1b). The forcing consists of monthly mean climatological atmospheric data. We introduce passive tracers injected into the main source water masses of the Arctic Ocean to study the spreading of these
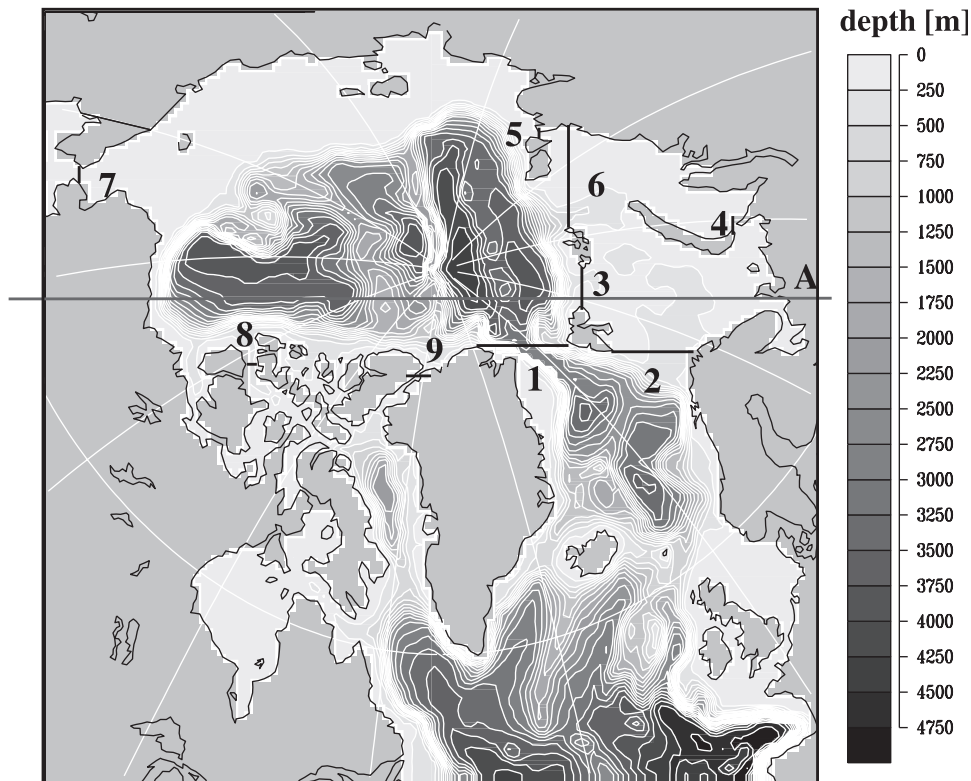
Figure 1. (continued)

tracers with the seasonal circulation patterns for interpretation and data comparison.

[6] After a brief introduction of the model the experiments are outlined. The presentation of the results starts with a description of the stratification and the seasonal circulation patterns of the surface, halocline, and Atlantic Water depths, followed by the results of the tracer experiments.

2. Model Layout and Experimental Design

[7] For the current investigation the coupled ice-ocean general circulation model Ocean Isopycnic Model (OPYC) [*Oberhuber*, 1993a] is set up to be integrated for several decades. The model consists of 14 layers of constant, prescribed potential density. It is based on the primitive equations and has a free surface. It employs the complete equation of state and a flux form for the dynamics. The potential densities of layers $2-15$ ($\sigma_\theta = 25.123$, 25.504, 26.832, 27.111, 27.345, 27.538, 27.694, 27.816, 27.909, 27.979, 28.021, 28.049, 28.062, and 28.066) are chosen to give a high resolution for the upper few hundred meters in the interior Arctic Ocean (Figure 2). Layer thicknesses are variable, and the layer interfaces are permeable for entrainment, detrainment, convection, and diapycnal mixing. A dual-entrainment scheme for diapycnal advection and diapycnal diffusion guarantees conservation of the vertical coordinates, which are fixed values for the potential densities. A mixed layer model at the surface (i.e., model layer 1) is coupled to a dynamic-thermodynamic ice model. The model mixed layer is governed by a bulk mixed layer approach in which the mixed layer depth is determined by a balance of buoyancy fluxes, potential and kinetic energy production, and dissipation. The approach allows detrainment and entrainment to occur from/into the isopycnal layers below the model mixed layer. We distinguish the model mixed layer from the "surface mixed layer," which is determined by the homogeneity of temperature and salinity. Thus, in case of detrainment the model mixed layer may

be shallower than the surface mixed layer. The coupled model is described in more detail by *Oberhuber* [1993a, 1993b, 1999], *Aukrust and Oberhuber* [1995], and *Holland et al.* [1996a, 1996b]. The version of the model used for the present study has open boundaries [*Kauker and Oberhuber*, 1997] and a finer horizontal
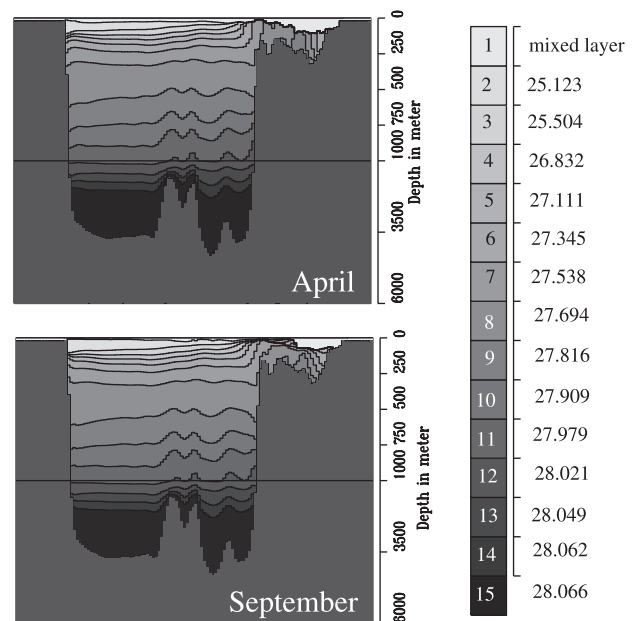
Figure 2. Vertical cross sections of the model layers in April and September of year 36. Layers 2–15 are equivalent to layers of constant potential density; layer 1 is the model mixed layer. For the location of the section see, line A in Figure 1b.

Table 1. Vertically Integrated Annual Mean Volume Transport (in Sverdrup) Through Key Sections in the Model Domain in Year 36[a]

Section	Transport North or East, Sv	Transport South or West, Sv
1. Fram Strait	1.5 (1.0–1.9)	3.4 (2.4–4.4)
2. Norway-Spitsbergen	2.6 (2.4–3.5)	0.3 (0.1–0.5)
3. Spitsbergen–Franz Josef Land	0.3 (0.2–0.5)	0.3 (0.1–0.5)
4. Kara Strait	0.5 (0.1–1.0)	· · ·
5. Vilkitsky Strait	0.2	· · ·
6. Franz Josef Land–Taymir	2.9 (2.4–4.0)	0.6 (0.3–0.8)
7. Bering Strait	0.8 (0.5–1.0)	· · ·
8. McClure Strait	· · ·	0.6 (0.5–0.8)
9. Nares Strait	· · ·	0.8

[a] The intervals in parentheses give the extreme values within the seasonal cycle. Please refer to Figure 1b for the location of the numbered sections.

and vertical resolution in contrast to *Holland et al.* [1996a, 1996b]. The mixed layer model provides coupling of the model ocean to ice and atmosphere. Mixed layer depth, temperature, and salinity are allowed to change freely according to the appropriate fluxes. Depending on the stratification of the upper ocean, the salt flux from ice during freezing periods may penetrate into the layers below the model mixed layer. The sea ice model works on the basis of a viscous plastic rheology [*Hibler*, 1979], however, written in flux form. A constant diffusion coefficient of 2000 m^2 s^{-1} for a Laplacian diffusion term has been applied in the ice momentum, mass, and concentration equations.

[8]   The horizontal resolution of the model is 0.5° in a rotated coordinate system, equivalent to ~50 km. The model domain covers the Arctic Ocean, the Nordic Seas, and the northern North Atlantic. Open boundaries are introduced at a latitude of about 50°N and in the Bering Sea where monthly mean values of temperature and salinity from *Levitus* [1982] are prescribed. The data from *Levitus* [1982] are also used for initialization. The sea level at the open boundaries is prescribed as well. It consists of a seasonal cycle of sea surface elevations derived from the T106 global version of the OPYC and an additional offset of +20 cm at the open boundary in Bering Strait relative to the northern North Atlantic. The offset tunes the Bering Strait throughflow to the observed annual mean of ~0.8 Sv [*Roach et al.*, 1995]. The formulation of the open boundaries is described in detail by *Kauker and Oberhuber* [1997] and *Cabos Narvaez et al.* [1998].

[9]   At the sea surface of the whole domain the salinity is restored to observed data on a timescale of 12 days. For this procedure a seasonal cycle of monthly means has been approximated by constructing a sinusoidal function with yearly period from observed summer and winter data from *Gorshkov* [1980] in the Arctic Ocean. Monthly mean data from *Levitus* [1982] have been used for the rest of the model domain. For the atmospheric forcing we constructed a climatological seasonal cycle from different data sets for the different parameters. Heat fluxes at the sea surface are derived from parameterizations [*Oberhuber*, 1993a] employing monthly mean climatological atmospheric temperatures of a European Centre for Medium-Range Weather Forecasts (ECMWF) analyses from the period 1985–1990 [*ECMWF*, 1988; *Aukrust and Oberhuber*, 1995]. The model is driven with climatological monthly mean ECMWF analysis wind stress data from the period 1980–1989 [*Trenberth et al.*, 1989]. Monthly mean climatological cloud cover and humidity are taken from *Wright* [1988]. The model topography is derived from the ETOPO5 data set by interpolation from the original 5′ × 5′ resolution to the model grid. Values for the Bering, Vilkitsky, Kara, and Fram Straits and the ridge height of the Lomonossov Ridge were corrected according to observed depths. The width of the McClure and Nares Straits of the Canadian Archipelago have been adjusted to a minimum width of two grid boxes to allow for a throughflow, the minimum depths being 150 and 200 m, respectively. The archipelago is closed otherwise.

[10]   The time step for ice and ocean models is half a day. For the horizontal eddy viscosity a harmonic formulation is used in combination with a diffusion coefficient that depends on grid size and deformation radii [*Oberhuber*, 1999], resulting in an eddy viscosity of the order of 5×10^3 m^2 s^{-1}. The diffusion coefficient for salt, temperature, and tracers is 250 m^2 s^{-1}.

[11]   The model is spun up for 35 years forced with the repeated climatological atmospheric seasonal cycle. By this time the fluxes through the main straits have adjusted, the vertically integrated volume flux through the gap Iceland-Norway shows interanual fluctuations of 1–4% around the mean. However, a thermodynamic equilibrium is neither reached nor intended for this study. The circulation of year 36 is interpreted and compared to observations. Table 1 shows the annual mean volume flows and their seasonal amplitude through the major straits. To analyze and visualize circulation and ventilation, passive tracers are injected to follow the incoming river water, the Bering Strait inflow water, and the Atlantic Water branches. The seasonal cycle of currents and layer distributions of year 36 is repeated for several decades to drive the tracer dispersion.

3.   Results and Discussion

3.1.   Temperature and Salinity

[12]   Vertical sections through the Arctic Ocean from the Alaskan coast to the Barents Sea show how the model hydrography adjusts to the 3.5 decades of prescribed atmospheric forcing (Figures 2 and 3). In the central basins, below the permanent ice cover, a strong halocline shields the cold and fresh surface mixed layer from the warm and salty Atlantic Water layer all year round. Here the thickness of a homogenous surface mixed layer varies between 20 and 150 m and can reach deeper than the model mixed layer (i.e., layer 1) (compare Figures 2a and 3). In the western Nansen Basin, however, a halocline is absent in winter. The isopycnals shoal steeply toward the Barents Sea slope and expose all density levels between $\sigma_\theta = 25.123$ (layer 2) and the upper Atlantic Water ($\sigma_\theta = 27.538$, i.e., layer 7) to the model mixed layer (Figure 2a). On the Barents Sea Shelf, even density layers 27.694 and 27.816 (i.e., layers 8 and 9) are in direct contact with the model mixed layer. In summer a low saline and relatively warm surface mixed layer develops, which extends southward from the Nansen Basin onto the northern part of the Barents Sea and isolates the dense layers.

[13]   Below the halocline a warm layer of Atlantic origin occupies the water column between 250 and 1000 m depth (Figure 3). Only in the western European Basin do the Atlantic Water layers reach up almost to the surface layer. The core of the FSBW branch of the inflowing Atlantic Water layer lies at about 300–500 m depth along the slope of the Siberian Shelves. North of the Barents Sea, its core temperature amounts to about 1.7°C; while it had a
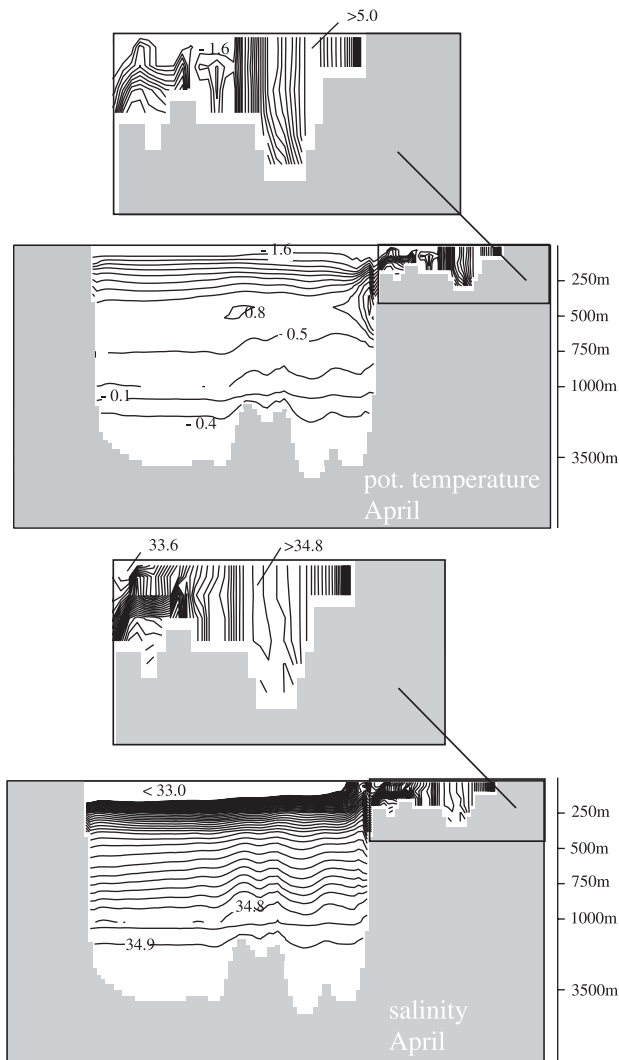
Figure 3. Vertical cross sections of (a) potential temperature and (b) salinity on a line between Alaska and the Barents Sea for the April of year 36. For the location of the section, see line A in Figure 1b.

temperature of 2.8°C when entering the Arctic through Fram Strait. The eastbound FSBW has a large width, and it covers the entire Nansen Basin. North of the Barents Sea, the core is still attached to the slope; it separates farther east and is replaced by colder and fresher water on the slope (Figure 4). Part of the FSBW enters St. Anna Trough on its western flank and recirculates northward on the eastern flank, experiencing freshening and cooling. Following the pathway of the two branches of Atlantic Water in the eighth layer ($\sigma_\theta = 27.694$) across the shelf (BSBW) and from Fram Strait along the shelf break (FSBW) (Figure 4) reveals the effect of the different ambient conditions on the temperature field. In contrast to the strong cooling of the BSBW, the FSBW is cooled only slightly between Fram Strait and the St. Anna Trough. Mixing of the warm and relatively salty main branch of FSBW and the fresher and colder products running from the shelf (dense BSBW and the recirculating branch of FSBW) takes place in the eastern European Basin. Farther downstream, gradients are very weak, and discrimination between the two components is difficult. The isolines suggest a broad recirculation of the FSBW in the eastern Eurasian Basin, a feature also observed by *Schauer et al.* [1996]. The part of the mixing product that is dominated by the FSBW and therefore relatively warm and salty occupies the interior eastern European

Basin stretching along the Lomonossov Ridge toward the North Pole. A local temperature and salinity maximum extends across the Lomonossov Ridge into the Makarov Basin (see the 0.9°C isotherm) comparable to data at 500 m depth from the climatology of *Gorshkov* [1980]. The near-slope part of the mixing product with lower temperature and salinity (not shown) is dominated by BSBW. It continues along the Siberian continental slope across the Lomonossov Ridge into the Makarov Basin. See also the results of the tracer experiment (Section 3.4) for an easier discrimination between FSBW and BSBW contributions in the Eurasian Basin.

[14] Temperature and salinity sections from the Barents Sea Shelf (zoomed figures in Figure 3) show the homogenization in late winter reaching down to the bottom in the southern part. Coldest temperatures close to the freezing point are found in a water column southeast of Spitsbergen. This feature is also visible in the potential temperature distribution of layer 8 (Figure 4) where low temperature patches indicate intense cooling.

3.2. Heat Fluxes

[15] The largest oceanic heat loss of several hundred W m^{-2} (monthly mean total heat fluxes) occurs in winter in the eastern Barents Sea, in Denmark Strait, and in the Labrador Sea (Figure 5a). Still considerable but less heat loss can be found in the West Spitsbergen Current (WSC) area and the interior Greenland Sea. From June to August in the entire domain the ocean gains heat from the atmosphere. Between June and September the mean total heat flux into the ocean in the Barents Sea is positive between 33 and 134 W m^{-2} (Figure 5b). These results show patterns similar to the total surface heat fluxes calculated by *Häkkinen and Cavalieri* [1989] on the basis of observed data. Their results for the anomalously cold year 1979, however, show a larger seasonal amplitude in the Barents Sea with up to 700 W m^{-2} loss just off the ice edge in February and more than 200 W m^{-2} gain in July. The modeled yearly mean heat loss in the Barents Sea amounts to ~47 W m^{-2} (76 TW), a value consistent with the net heat influx into the Barents Sea from the large-scale circulation model of *Gerdes and Schauer* [1997]. The value is about half of the estimate from *Simonsen and Haugan* [1996] of 98–112 W m^{-2} (149–174 TW), which is based on oceanic transport observations and an optimiza-
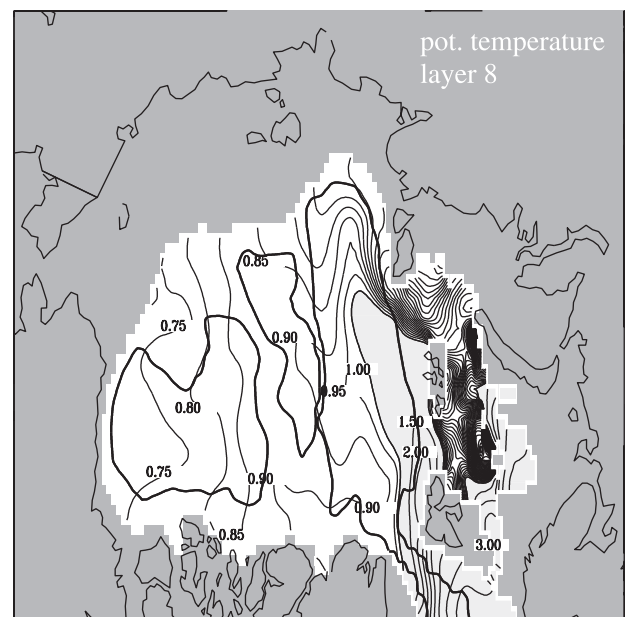

Figure 4. Potential temperature on model layer 8 in year 36 of the model integration. Temperatures above 1°C are shaded. The thick line depicts the 2500 m depth contour.
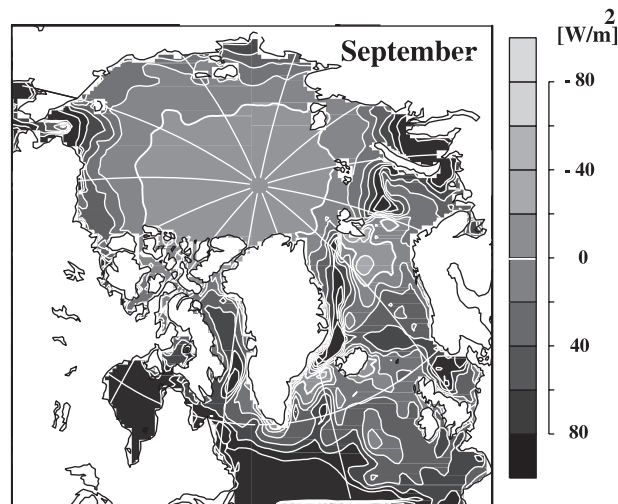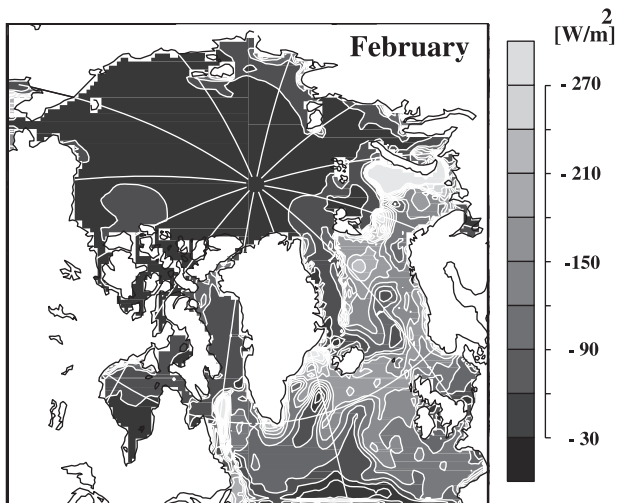
Figure 5. The ocean surface heat flux in (a) February and (b) September in W m^{-2}. The thick white line equals zero heat flux.
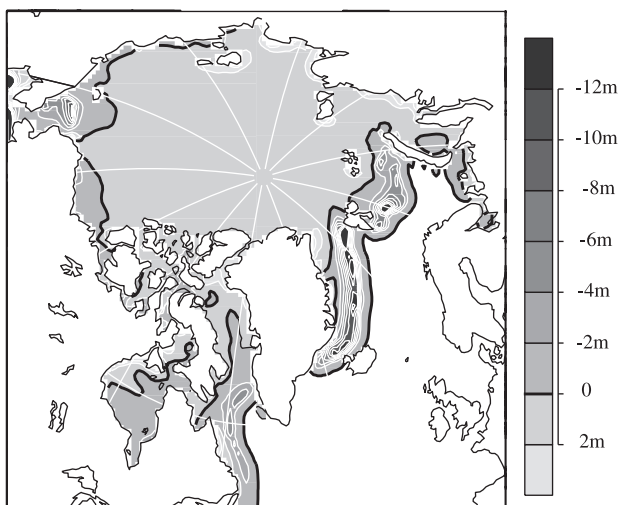

Figure 6. The yearly sum of ice melt and freeze in meters as diagnosed from year 36.

tion of heat flux parameterizations from the entire Nordic Seas and the Arctic Ocean.

[16] A further source for densification and eventual homogenization is the brine release due to ice formation in areas of large heat loss. The model produces a seasonal melting and freezing cycle with areas of most intense winter freezing of up to 2 m per month at the coasts of the Kara Sea, the Laptev Sea, and Alaska. While in the annual mean a large area shows net freezing, there is net melting only along the marginal ice zones, with maxima above 12 m net melt per year in the Barents Sea, the Greenland Sea, and the Chukchi Shelf and 2–5 m in the Labrador Sea (Figure 6).

3.3. Circulation and Water Mass Modification

3.3.1. Circulation of mixed layer and ice.

[17] Throughout the year the circulation at the surface of the central Arctic Ocean is characterized by a strong, meandering TPD (Figure 7). The TPD consists of a Canadian branch, moving from the Bering Strait toward the pole, and a Siberian branch, which is fed by the surface
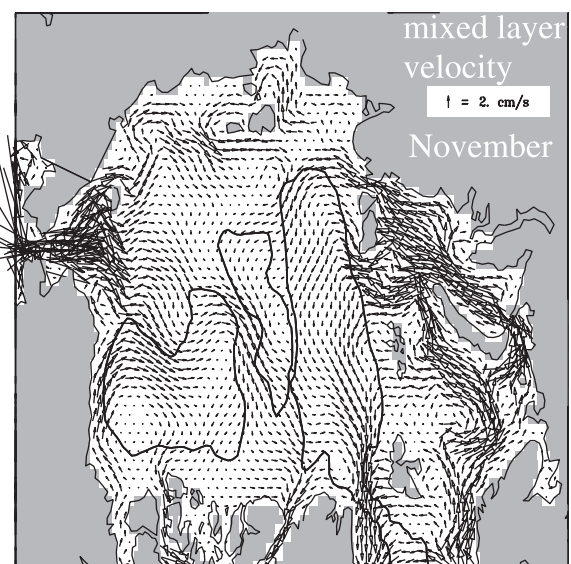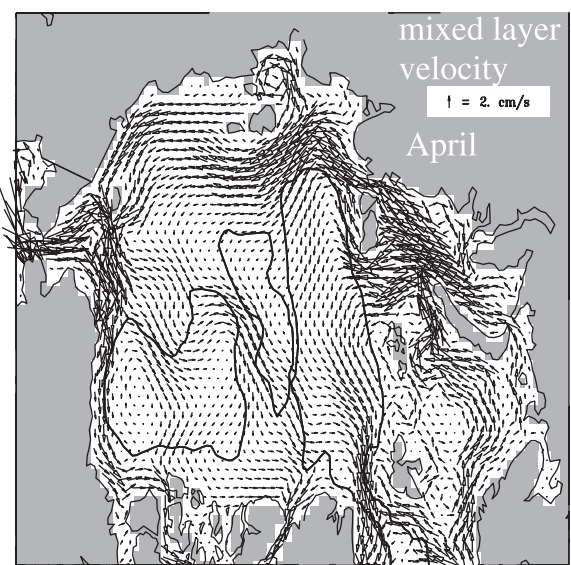

Figure 7. Velocity in the model mixed layer in (a) April and (b) November of year 36. The thick line depicts the 2500 m depth contour.
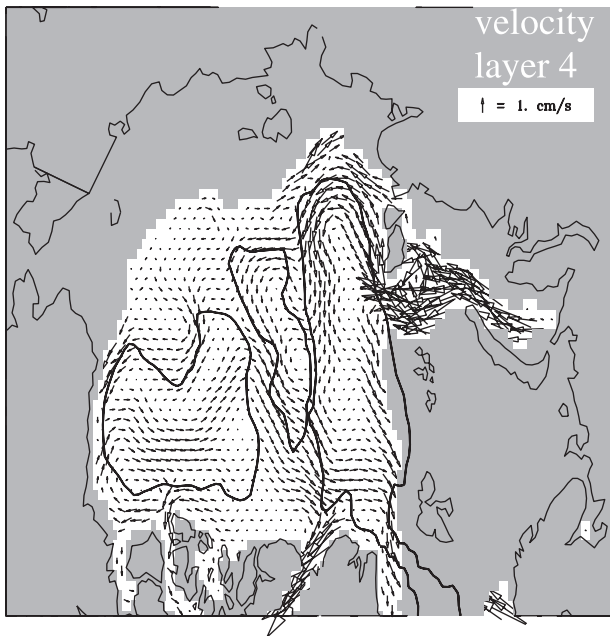
Figure 8. As in Figure 7 but for model layer 4 in April. This layer represents the model's lower halocline. In the shaded areas beyond the coastline the layer is not existent, i.e., has a thickness equal to zero.

waters leaving the shelves of the Barents, Kara, and Laptev Seas. Part of the water entering through Bering Strait feeds directly into the TPD's Canadian branch. On the eastern Siberian and the Alaskan Shelves the surface flow is seasonal. From late winter to early summer an eastward coastal current develops along the Siberian Shelves from the Kara Sea to the East Siberian Sea, driven by the salinity gradient due to river runoff, while in late summer and early winter the eastern Siberian Shelf is flushed with part of the Bering Strait water that flows westward along the Chukchian Shelf. The oceanic Beaufort Gyre weakens and detaches from the North American coast in late winter and spring to give way for an eastward extension of the Bering Strait inflow, and in summer it is absent. Such a detachment of the anticyclonic Beaufort Gyre is visible also in other numerical models of the Arctic Ocean for different forcing fields [e.g., *Häkkinen and Mellor*, 1992; *Maslowski et al.*, 2001].

[18] A strong eastward flow entering the Barents Sea Shelf from the Norwegian Sea dominates the circulation in the Barents, Kara, and Laptev Seas and is stable throughout the year. An exception is a sluggish westward flow in the inner Kara Sea in summer, as shown in a regional study from *Harms and Karcher* [1999]. In contrast, the WSC has a strong seasonal cycle, strongest from March to May.

[19] The lower part of the surface mixed layer ($\sigma_\theta = 25.123$, i.e., layer 2) is fed with the inflow through Bering Strait and by water detrained from the model mixed layer (not shown). The water of Pacific origin also spreads eastward toward the Canadian Archipelago. Water of Atlantic origin leaves the Kara Sea through the Vilkitsky Strait into the Laptev Sea. From here it spreads into the Canadian Basin and northward to the Amundsen Basin. The water exits the Arctic Ocean mainly through the Canadian Archipelago and, a small amount, through Fram Strait.

[20] The oceanic freshwater export through Fram Strait, which concentrates in the upper 200 m of the water column, amounts to 1270 km^3 yr^{-1}, relative to a reference salinity of 34.8. Comparing these numbers with observations, one has to keep in mind, however, that the model sea surface salinity is restored to climatological data on a timescale of weeks. Thus the lateral

freshwater fluxes are also rather tightly bound to the integral of these data.

[21] The drift pattern of the sea ice reveals a large Beaufort Gyre above the entire Canadian and Makarov Basins in winter (not shown). In summer the ice drift changes into a very weak cyclone over the Beaufort Sea. While in summer a TPD in the ice drift still exists the ice export from the Kara and Laptev Seas stops, commencing again in October. The ice thickness is at maximum north of the Canadian Archipelago and Greenland with about 8 and 4–5 m in the central Arctic in winter. The annual mean ice export through Fram Strait amounts to 0.10 Sv. This is in good agreement with an average ice export rate of 0.11 Sv, which was found by *Gerdes* [2000] when driving the model of *Gerdes and Köberle* [1999] with atmospheric conditions from 1979–1993. It also agrees with observations from *Vinje et al.* [1998], who found an export of 0.09 Sv for the period 1990–1996.

3.3.2. Circulation of halocline water. [22] The halocline (layers 3–5, $\sigma_\theta = 25.504–27.111$) receives a strong inflow from the Siberian Shelves, mainly from between Franz Josef Land and Svernaya Semlya (Figure 8). In accordance with *Rudels et al.* [1996] the interior circulation of the lower part of the halocline is very similar to the Atlantic Water (AW) circulation with several cyclonic recirculation gyres in the Eurasian and Canadian Basins. The halocline water exits the Canadian Basin by crossing the Lomonossov Ridge between Greenland and the North Pole. In western Fram Strait the halocline water leaves the European Basin with the East Greenland Current.

3.3.3. Circulation of Atlantic Water. [23] The model circulation in the depth interval between 200 and 1000 m (model layers 6–11, $\sigma_\theta = 27.345–27.979$) is dominated by several cyclonic cells in the Eurasian and Canadian Basins. A similar flow pattern has been pointed out by numerous authors after *Rudels et al.* [1994]. In the western European Basin, where no halocline is present and the isopycnal layers shoal upward (Figure 2), the strong inflow of FSBW with the WSC feeds a cyclonic circulation. It is augmented with BSBW, which runs off the Kara Sea Shelf and forms the outer branch of the cyclonic flow (Figure 9).

[24] FSBW and BSBW follow the Siberian slope to the Lomonossov Ridge. Here part of the FSBW on the inner branch of the cyclonic flow recirculates poleward along the Lomonossov Ridge
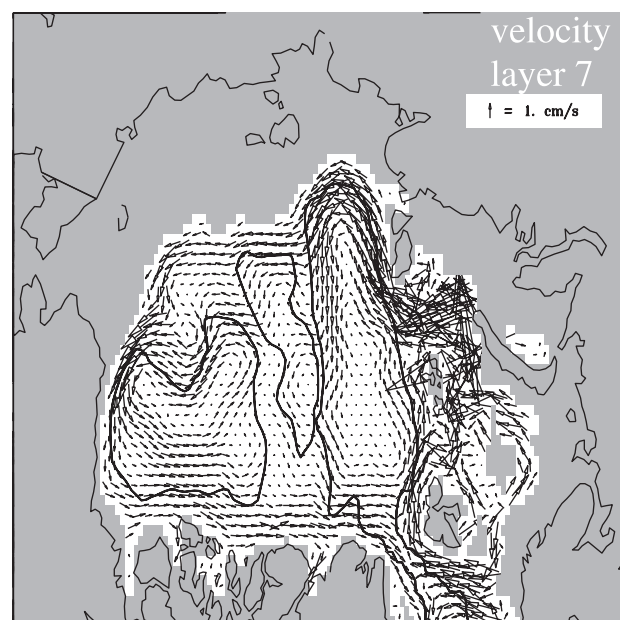

Figure 9. As in Figure 8 but for model layer 7. This layer represents the model's upper AW.

Net flow Barents Sea Opening
(Spitsbergen - Norway)

Net flow fromBarents Sea to central Arctic
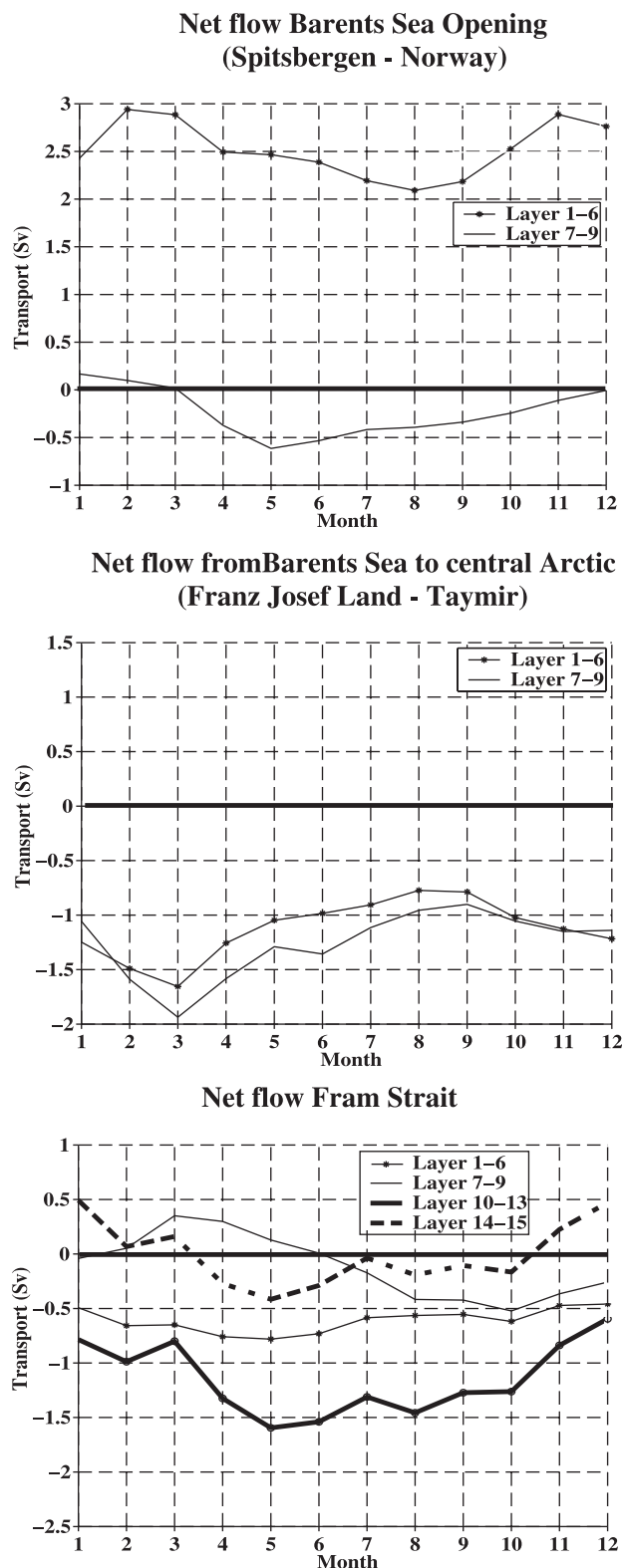### (Franz Josef Land - Taymir)

Net flow Fram Strait

Figure 10. The net inflows and outflows of volume for the Barents Sea at two different density classes across the sections (a) Spitsbergen-Norway, (b) Franz Josef Land-Taymir, (positive into the Barents Sea), and (c) the net flow of volume across Fram Strait at four different density classes (positive into the Arctic Ocean). The data are monthly means from year 36. For an identification of potential densities from the layer numbers compare with the list of potential densities given in Figure 2.

and crosses it into the Makarov Basin. Here it runs southward as a return flow on the eastern flank of the ridge, which explains the temperature maximum in the Makarov Basin at the AW depths (Figure 4). A similar return flow of water from the European Basin on the eastern flank of the Lomonossov Ridge has been deduced from hydrograhic observations by *Schauer et al.* [2002] and has been attributed partly to the existence of seamounts on top of the ridge, promoting anticyclonic flow to cross the ridge. The grid resolution used in this study, however, is much too coarse to incorporate such small-scale topography. The results shown here indicate instead that the observed flow pattern is well supported even by the large-scale topography of the ridge.

3.3.4. Water mass modification. [25] As pointed out before, in the Barents Sea, part of the intruding AW is modified into the denser BSBW, which subsequently leaves the shelf through the gap between Franz Josef Land and the Taymir peninsula toward the European Basin. The consequences of this process are depicted in Figures 10a and 10b, which compare the volumes of two potential density classes when entering and leaving the Barents Sea. The largest density that is produced on the Barents Sea Shelf ventilates model layer 9 (σ_θ = 27.816). Densities have been subdivided into a light class covering layers 1–6 (σ_θ = 27.345) and intermediate dense water encompassing layers 7–9 (σ_θ = 27.538–27.816). The flow through Franz Josef Land to the Spitsbergen section is small and approximately balanced and thus does not contribute to the balance of inflows and outflows of the Barents Sea. The inflow of water from the Nordic Seas into the Barents Sea across the line Spitsbergen-Norway (Figure 10a) mainly consists of lighter water in layers 1–6. Maximum inflow at these densities occurs in wintertime; minimum inflow occurs in summertime. Denser water contributes only little to the flow across this line, with a net inflow in January and February; while in the rest of the year a small outflow of up to 0.6 Sv takes place to the Nordic Seas. At the section between Franz Josef Land and Taymir (Figure 10b) a net outflow is apparent all year, with almost equal contributions of the light densities (layers 1–6) and the intermediate dense water (layers 7–9), which make up the BSBW. The outflow of the latter has a well-defined seasonal peak of almost 2 Sv of outflow to the deep basins in March. In late winter (February–May) this layer has direct contact to the model mixed layer above the shallow Central Bank in the Barents Sea, where it experiences cyclonic rotation. This phenomenon is depicted by the vertical section of potential densities in Figure 2. Running downslope, this very cold water fills the deep troughs in the central Barents Sea. From May to October, when no new dense water is supplied by the model mixed layer, the rotation changes to anticyclonic. While the Central Bank in the Barents Sea is well known for the production of dense bottom water [e.g., *Quadfasel et al.*, 1992], its further path has been questioned. *Quadfasel et al.* [1992] deduce a drainage to the Norwegian Sea from hydrographic sections taken in 1983. We can find no indication for such a path in our results. As a bottom plume of up to 100 m thickness, the densest

Table 2. Volume Flow of Arctic Rivers Used in the Model Study[a]

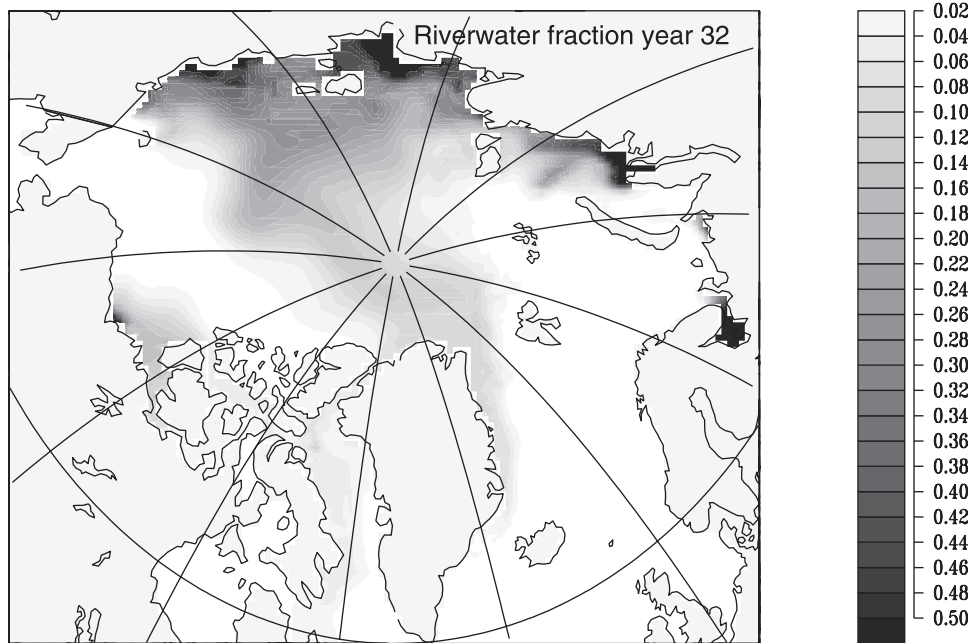| Rivers	Flow, km³ yr⁻¹
Voronja and Severnaja Dvina	114
Mesen and Pechora	158
Ob and Pur	563
Yenisey and Pjasina	689
Nishnya Taymira	35
Katanya and Anabar	130
Oljenok and Lena	560
Yana	38
Indigirk	57
Anaseja and Kolima	112
Mackenzie	340

[a] From *Treshnikov* [1985].

Figure 11. River water fraction at the surface after 32 years of release of a passive river water tracer. The tracer has been injected at the estuaries of the 18 major Arctic rivers according to the climatological mean seasonal runoff cycle from the atlas of *Treshnikov* [1985].

water flows northeastward toward St. Anna Trough and, with a smaller branch, to the Victoria Channel between Spitsbergen and Franz Josef Land, feeding the near slope AW layer.

[26] Across Fram Strait the second entrance to the Arctic Ocean proper and gate for the FSBW, intermediate densities (layers 7−9) and bottom water densities (layers 14 and 15, $\sigma_\theta = 28.062$) show seasonally changing sign of inflow/outflow (Figure 10c). A net flow out of the Arctic Ocean occurs at the lightest densities (layers 1−6) and the deep water densities (layers 10−13, $\sigma_\theta = 27.909$−28.049) all year long, with a maximum outflow in late spring. A further densification of AW along its path in the Arctic basins becomes evident when comparing the net flows to layers 7−9 from the shelf (Figure 10b) and the net outflow to the Nordic Seas across Fram Strait, which takes place dominantly at the deep water density class (layers 10−13).

[27] To get better the picture for the entire Arctic Ocean, we sum up for yearly mean balances of volume flow across all inflows and outflows to the Arctic Ocean, including the the Canadian Archipelago and the Bering Strait. A net amount of 1.4 Sv is densified on the Barents/Kara Sea Shelf from 2.5 Sv of inflowing light (layers 1−6) to intermediate (layers 7−9) density. Of this intermediate dense water a net 0.2 Sv are running off to the Nordic Seas, while 1.2 Sv are fed into the intermediate density layers (7−9) of the Arctic Ocean. A net 1.1 Sv of this water in turn is converted to the next larger densities (layers 10−13) and leave the Arctic Ocean via Fram Strait.

3.4. Tracer Experiments

[28] For the following experiments passive conservative tracers have been injected at different locations to be advected and diluted over several decades. The choice of input locations for the tracers has been chosen such that each of the experiments may represent a different water mass. The pathways and dilution of the tracers reveals important information on how each of the water masses ventilates the upper and intermediate Arctic Ocean in the model.

3.4.1. River water tracer. [29] Since the model does not have an explicit inflow of river water, the inflow of freshwater on the shelves is realized via restoring the sea surface salinity to observed salinity data for summer and winter. To analyze the spreading of river water, a passive tracer is injected in proportion to the observed climatological monthly mean river runoff from the atlas of *Treshnikov* [1985] at the locations of the major 18 Arctic rivers. See Table 2 for the names and yearly runoff. After about 3 decades the tracer distribution is in approximate equilibrium.

[30] The major amount of river water stems from the rivers Ob and Yenisey, entering the Kara Sea, and the river Lena, feeding the Laptev Sea. The Ob and Yenisey waters exit the Kara Sea near Svernaya Semlya and through Vilkitsky Strait, where the major fraction passes, in agreement with results from *Frank* [1996], who derived river water fractions from $\delta^{18}O$ measurements (Figure 11). East of the strait, the Kara Sea river water joins the Lena river water. The river water plume penetrates far eastward onto the East Siberian Shelf. Between here and the Laptev Sea it leaves the shelves and penetrates far into the Canadian Basin until it is carried toward Fram Strait with the TPD. The plume with the maximum river water fraction crosses the Lomonossov Ridge to reenter the European Basin near the Morris Jessup Plateau. A smaller fraction enters Nares Strait. Finally, the river water moves toward Fram Strait approaching from the Canadian Basin. The distribution of the river water fractions reflects the fact that the upper layers of the model advect water from the Canadian Basin to the western Eurasian Basin in a similar fashion as described by *Rudels et al.* [1996]. In the western Eurasian Basin the maximum fraction of river water in the polar surface mixed layer amounts to 10−14%, which is in accordance with the fractions derived from $\delta^{18}O$ measurements [*Bauch et al.*, 1995] for this area. The water of the Mackenzie River exits the central Arctic eastward and southward through the Canadian Archipelago. *Guay and Falkner* [1997] hypothesize high Barium concentrations in the central Canadian Basin surface waters to be indicative of Mackenzie River Waters. Instead, our model experiments show that the Mackenzie River tracers are confined to the southern Beaufort Sea and that no injection into the interior Candian Basin takes places. One reason for this discrepancy may be that the interannual variability of the circulation in the Canadian Basin surface waters is because of the use of a climatological forcing in our study. We assume that an
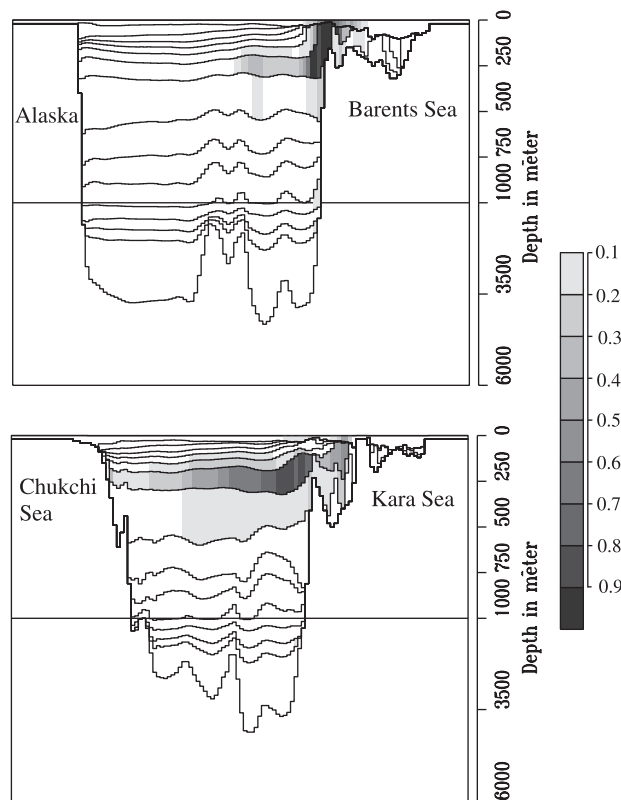
Figure 12. Concentration of the FSBW tracer on vertical cross sections (a) from Alaska to the Barents Sea (section A in Figure 13) and (b) from the Chukchi Shelf to the Kara Sea (section B in Figure 13). The isohalines depict the interfaces of the model layers 1–15.

interannually variable position and extension of the Beaufort Gyre may promote a mixing or even advection of Mackenzie River Water into its center.

[31] The advective timescale for the river water in the model is 2–3 years on the shelves and 12–14 years to reach Fram Strait. *Schlosser et al.* [1994] estimated a mean residence time of 3.5 ± 1.5 years for the river water on the shelves from the difference of tritium /³He age and tritium vintage age. Three and a half years have also been estimated by *Pavlov and Pfirman* [1995]. The mean residence time of river water in the polar surface layer of the Eurasian Basin based on $\delta^{18}O$ measurements and river water volume balances is computed to 4.1–6.5 years by *Frank* [1996]. Values estimated for the entire Arctic Ocean area, including the shelves, vary from 10 ± 1 years [*Östlund and Hut*, 1984] to 11–14 years [*Bauch et al.*, 1995].

3.4.2. FSBW and BSBW tracers. [32] The two components of Atlantic origin enter the Arctic as the FSBW and the BSBW [*Schauer et al.*, 1996]. To trace these two water masses separately, we provided the model with a tracer concentration of unity from the top to the bottom on two sections between Franz Josef Land and Taymir across the St. Anna Trough for the BSBW and between Spitsbergen and Greenland for the FSBW. The model flow determines by which layer and in which direction the tracer will be advected.

[33] At the surface the FSBW tracer is advected eastward into the European Basin by the WSC. Approaching the longitude of Franz Josef Land, the surface concentrations reduce drastically as a result of subduction under the cold and fresh Polar Surface Water. The vertical section just east of Spitsbergen (Figure 12a) shows that in the eastern European Basin the FSBW is still in contact with

the model mixed layer at the surface, whereas east of Franz Josef Land, it is covered by the model mixed layer and the halocline (Figure 12b). The covering of the FSBW with Polar Surface Water at an eastern longitude as far as Franz Josef Land is consistent with observations of *Rudels et al.* [1996]. The contact of halocline and upper Atlantic Water layers (less than layer 7) with the model mixed layer allows the exchange of properties between mixed layer and Mthe deeper layers. Consistent with this situation is the enhanced surface heat loss north of Spitsbergen in excess of 30 W m^{-2} in winter (Figure 5a) and weaker ice cover in winter as compared to the northern and eastern adjacent areas (not shown). Continuing its passage at depth in the Arctic Basins, the major portion of the FSBW tracer travels in the seventh model layer ($\sigma_\theta = 27.538$) between 150 and 250 m depth. The water needs 6–8 years to cover the distance between Fram Strait and the intersection of the Lomonossov Ridge with the continental slope north of the Laptev Sea. Here part of the water recirculates toward Fram Strait along the ridge, reaching the strait about 15–20 years after release.

[34] The recirculation starts already north of the confluence area, as was deduced by *Schauer et al.* [1996] from temperature distributions in the interior European Basin. The remaining part continues into the Makarov Basin, where it follows the depth contours of the continental slope to reach the Chuckchi Plateau about 15 years after its start and Fram Strait after ∼30 years (Figure 13). These advective timescales agree very well with the transit times derived from observed tracer distributions by *Smethie et al.* [2000]. They find about 7 years of transit time for the BSBW from the entrance of the Barents Sea to the Lomonossov Ridge-continental slope intesection. They derive a travel time of about 14 years to the area north of Greenland along Lomonossov Ridge and about 18 years for the branch that entered the Makarov and Canadian Basins along the continental slope to reach the Beaufort Sea.

[35] When the AW reaches the continental slope of the Kara Sea after a shelf passage of 2–3 years, the water has experienced strong interaction with river water, intense cooling, and ice formation on the shelf. It continues in the form of three varieties traceable in the BSBW tracer distributions. The lightest water leaves the shelf in the polar surface mixed layer, feeds the Siberian branch of the TPD, and reaches Fram Strait after 3–6 years. About 10 years after the start of the tracer release the distribution of the tracer concentrations in the polar surface mixed layer have reached a steady
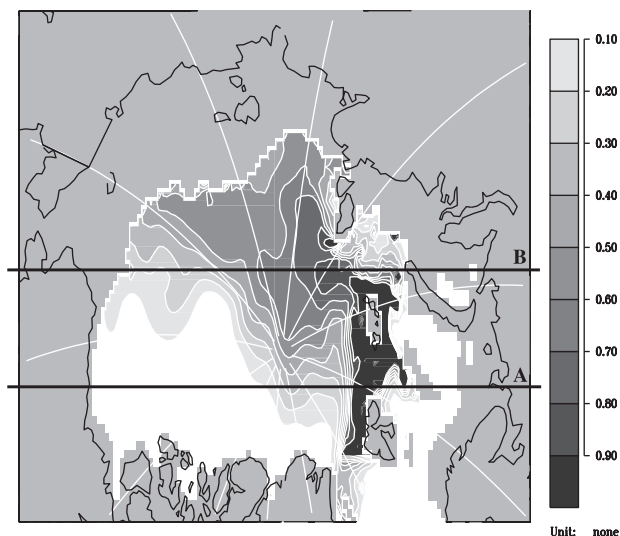

Figure 13. Concentration of the FSBW tracer in layer 7, which carries the major portion of the FSBW, 15 years after start of the release.
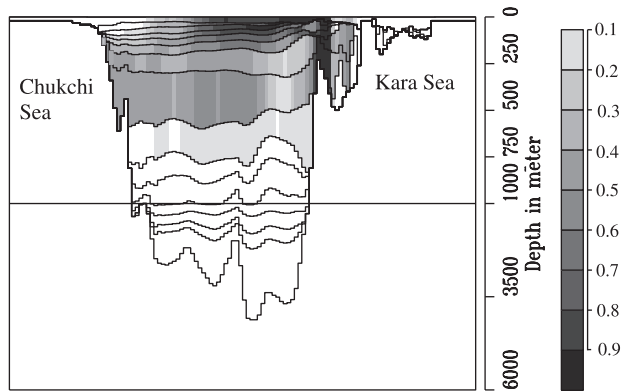
Figure 14. Concentration of the BSBW tracer in the model layers on a vertical cross section from the Chukchi Shelf to the Kara Sea (section B in Figure 15).

state. The water in the medium density range $\sigma_\theta = 25.504-27.111$ (layers 3–5) feeds the halocline. The high concentrations of BSBW tracer in the halocline water of the European Basin (Figure 14) reveal the contribution of the Barents Sea to the formation of the model's halocline water. The concentrations of FSBW tracer, on the other hand, are comparatively low in the halocline. The densest variety of BSBW (>27.538) slides down the slope to within the eighth and to a smaller extent within the seventh and ninth model layers. Here the BSBW pushes the FSBW off slope, forming the lower, denser part of the AW in the interior Arctic Ocean. The tracer concentrations of the two sources reflect this in the eastern European Basin (Figures 13 and 15). Whereas the concentration of the BSBW and FSBW tracers are approximately equal in the seventh layer, representing the upper AW, the relation of BSBW tracer to FSBW tracer concentrations in the eighth layer is about 2:1. This is similar to what *Schauer et al.* [1996] report from the eastern Eurasian Basin as a result of hydrographic measurements: a fraction of 50% FSBW:50% BSBW and 80% BSBW:20% FSBW for the upper and lower Intermediate Water, respectively. Again, in the model the recirculation pattern and advection timescales of the BSBW tracer at depth are similar to the FSBW tracer; however, the latter moves on an inner loop, while the BSBW tracer moves closer to the slope.
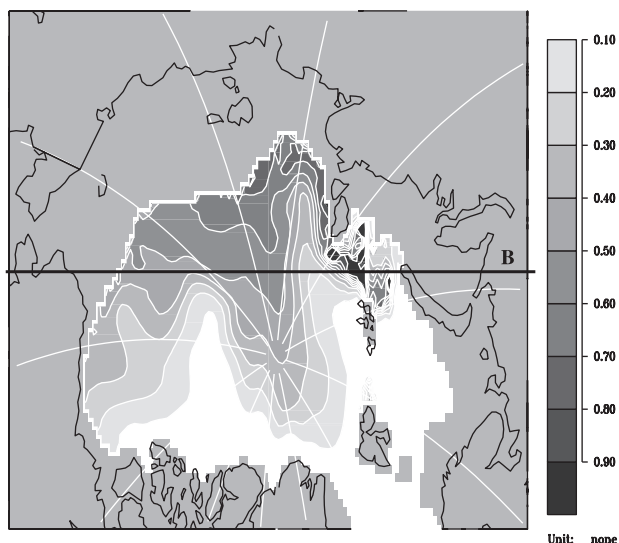

Figure 15. Concentration of the BSBW tracer in layer 8, which can be identified as the model's lower AW layer.
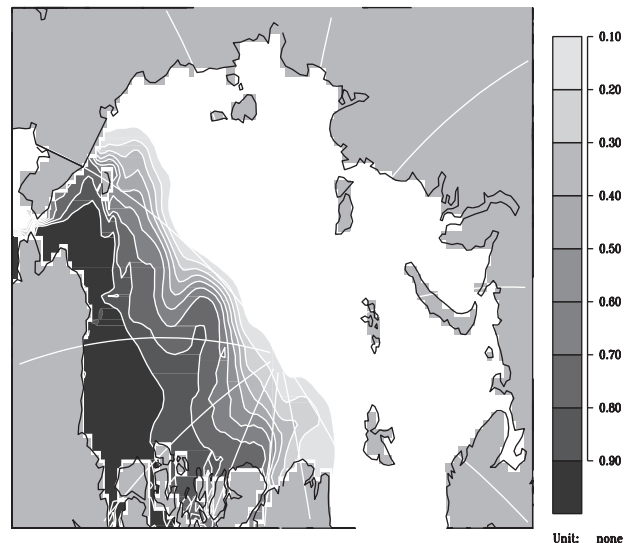

Figure 16. Surface concentration of Bering Strait inflow tracer in year 30 after the start of the release.

[36] The model results for the travel times correspond to values deduced from hydrographic [*Schauer et al.*, 1996] and tracer measurements [*Frank et al.*, 1998; *Smethie et al.*, 2000]. These investigations point to mean current speeds of about 1 cm s^{-1} for the two branches in the Nansen Basin, consistent with an apparent tracer age of the FSBW of 2 years north of the Barents Sea and 6 years north of the Laptev Sea and 1 year south of Fram Strait.

[37] Our results contradict, however, travel times for the European Basin deduced by *Swift et al.* [1997], which are based on current measurements from the WSC (10 cm s^{-1}), the Siberian slope (8 cm s^{-1}),and the Lomonossov Ridge (2 cm s^{-1}). Their estimated travel times are 1 year from west of Spitsbergen to Svernaya Semlya and 3–4 years to the North Pole along the continental slope and the Lomonossov Ridge in the European Basin.

3.4.3. Bering Strait Water tracer. [38] The inflow of water through Bering Strait pulsates in a seasonal cycle with maxima in winter. While the minor branch moves westward onto the East Siberian Shelf, the major one carries Pacific Water toward Fram Strait following the North American coastline. Consequently, the largest concentrations are found in the southern Beaufort Sea (Figure 16). The water leaves the Arctic Ocean through the Canadian Archipelago. Only a small fraction is carried as far east as Fram Strait, giving rise to surface tracer concentrations of 0.1.

4. Summary and Conclusions

[39] To investigate the replacement and ventilation of the upper and intermediate depths of the Arctic Ocean, a version of the coupled ice-ocean genearl circulation model OPYC is set up. It is driven with a climatology of monthly means of atmospheric data from the 1980s. The model shows a dominating cyclonic movement for the intruding water masses of Atlantic origin, the river water, and the Pacific Water entering through Bering Strait. The drift of ice and water show a strong seasonality with maximum changes of the ocean currents along the perimeter of the Arctic Ocean. The circulation of the surface waters north of the Canadian Archipelago and in the western European Basin is distinct from the movement of the winter ice cover, while ice and water move similarly in the rest of the domain. The cyclonic tendency of the summer ice drift and the eastward spreading of the Bering Sea and Mackenzie River Water tracers found in these experiments are typical features for years that are dominated by a cyclonic

atmospheric pressure regime in the Arctic [*Proshutinsky and Johnson*, 1997], as shown in a model study by *Polyakov et al.* [1999]. The eastward spreading of Bering Strait Water also corroborates the findings from *Jones et al.* [1998], who suggest a two-branch movement of Pacific Water in the Arctic, interpreting the distribution of water mass concentrations in a composite chart with data from 1983 to 1996.

[40] Water of Atlantic origin enters in two branches through Fram Strait and via the Barents Sea Shelf. We found the mixed layer of the European Basin being ventilated with modified AW from the Barents Sea and northern Kara Sea Shelves. At the surface, part of the water on the shelf becomes fresher because of a mixture of melt and river water, which is parameterized by a restoring to observed salinities. This surface water crosses the European Basin and intrudes far into the Canadian Basin, forming a front with Bering Strait-derived water over the Alpha-Mendeleyev Ridge, as can be visualized by the passive tracer experiments.

[41] Also, for the halocline water the Barents Sea and northern Kara Sea Shelves are ventilation source areas, while the inflow from Fram Strait only plays a minor role. In the western European Basin a halocline is absent. Instead, the isopycnals shoal southward, and, layers 3−7 are in contact with the model mixed layer. This means that in this area each of the density layers that form the halocline and the upper AW in the remaining part of the Arctic Ocean may exchange properties directly with the model mixed layer. This finding agrees with the idea of *Rudels et al.* [1996] that part of the lower halocline water may be formed in the western Nansen Basin from ice formation and melting.

[42] Below the halocline, AW layers that are fed by the FSBW and the BSBW move along cyclonic gyres in the European and Canadian Basins in a fashion similar to that described by *Rudels et al.* [1994]. Concurrent with *Swift et al.* [1997], we find the boundary currents playing a major role in the transport of ventilated water from the shelf and slope areas into the interior Arctic Ocean. The crossing of Lomonossov Ridge by the AW happens in two branches. The first branch flows along the shelf slope of the Laptev Sea at the intersection of ridge and slope. The second branch twists off from the cylconic gyre in the Eurasian Basin farther north, crosses the ridge as a broad flow, and feeds into a southward return flow on the eastern flank of the ridge. Such a flow pattern has been suggested also by *Schauer et al.* [2002] on the basis of hydrographic observations.

[43] The travel times of the boundary flows calculated in this investigation match with observations [*Smethie et al.*, 2000]. The AW exits Fram Strait 15−20 years after entering the Arctic Ocean, taking the short, inner loop along the Lomonossov Ridge, and after at least 30 years, taking the long, outer loop along the continental slope. For river water in the surface mixed layer we find 12−14 years of travel time from the river mouths to Fram Strait, in agreement with values calculated from tracer observations [*Bauch et al.*, 1995; *Frank*, 1996]. The model gives evidence that the BSBW seems to be the more relevant branch for the lower AW layer. It is an end product of AW that has passed the area west of Nowaja Semlja on the Barents Sea Shelf where it has been exposed to extreme heat loss during its 1−2 year passage. It provides the dominant volume input for the lower part of the AW. This supports the conclusions *Schauer et al.* [1996] drew from an interpretation of hydrographic measurements. The yearly mean net production of water with densities in access of $\sigma_\theta = 27.538$ on the shelves of the Barents and Kara Seas is 1.2 Sv. The major part of this water experiences further densificiation on its path in the Arctic Ocean proper to Fram Strait, resulting in a net export of 1.1 Sv of densities in excess of $\sigma_\theta = 27.909$.

[44] The model experiment reveals a vigourous inflow of AW into the Makarov Basin. Such a feature has been deduced from observed CFCs [*Carmack et al.*, 1997] and ^{129}I [*Smith et al.*, 1999; *Karcher et al.*, 1999] in the Canadian and Makarov Basins from the

early 1990s. In these years the Atlantic/Pacific Water frontal zone from the Lomonossov Ridge toward the Mendeleev Ridge is shifted relative to its position in the 1970s [*Swift et al.*, 1997; *McLaughlin et al.*, 1996].

[45] The similarity of the model results with the observations may be astonishing since the model has been driven for 3 decades with an atmospheric climatology from the 1980s. It reflects, however, the importance of the upstream conditions for the AW Layer in the Arctic Ocean. While the regional atmospheric fields certainly play the major role for the wind stress field and the local surface fluxes [*Proshutinsky and Johnson*, 1997; *Polyakov et al.*, 1999], the AW conditions below the halocline are influenced to a large extent by the lateral boundary conditions, namely the intensity, temperature, and salinity of the two inflowing Atlantic branches entering through Fram Strait and the Barents Sea. These in turn are dependent on the atmospheric state in the source areas, the northern North Atlantic and the Nordic Seas [e.g., *Grotefendt et al.*, 1998; *Dickson et al.*, 2000]. From the model results shown here and from observations we can assume an advective timescale for the propagation of anomalies in the AW of 5−10 years from the Nordic Seas to the eastern Eurasian Basin. The high North Atlantic Oscillation (NAO) index state in the 1980s and 1990s coincided with a warmer and stronger inflow into the Arctic Ocean [*Dickson et al.*, 2000], the advective signal of which would appear 5−10 years later in the eastern Eurasian Basin.

[46] The question of the relative importance of the upstream conditions, namely the high NAO state of the late 1980s/early 1990s and the long cyclonic regime of the Arctic sea level pressure from 1980 to 1997 [*Proshutinsky and Johnson*, 1997] for the frontal shift in the early 1990s, could not be answered here. This will be the task of future numerical experiments with variable atmospheric forcing. The same holds for an investigation on the dependence of the BSBW and the densified end product on the variability of the advectice boundary conditions like temperature and salinity in Norwegian Atlantic Current, the Norwegian Coastal Current, and river water. In addition to the features of the model used here, an inclusion of explicit time-dependent river runoff without restoring of sea surface salinity and the incorporation of the Nordic Seas as part of the model domain are essential ingredients to tackle these tasks.

References

Aagaard, K., L. K. Coachman, and E. C. Carmack, On the halocline of the Arctic Ocean, *Deep Sea Res., Part A*, *28*, 529–545, 1981.

Anderson, L. G., E. P. Jones, and B. Rudels, Ventilation of the Arctic Ocean estimated by a plume entrainment model constrained by CFCs, *J. Geophys. Res.*, *104*, 13,423–13,429, 1999.

Aukrust, T., and J. M. Oberhuber, Modelling of the Greenland, Iceland, and Norwegian Seas with a coupled sea ice-mixed layer-isopycnal ocean model, *J. Geophys. Res.*, *100*, 4771–4789, 1995.

Bauch, D., P. Schlosser, and R. G. Fairbanks, Freshwater balance and the sources of deep and bottom waters in the Arctic Ocean inferred from the distribution of H$_2^{18}$O, *Prog. Oceanogr.*, *35*, 53–80, 1995.

Cabos Narvaez, W., M. J. OrtizBevia, and J. M. Oberhuber, The variability of the tropical Atlantic, *J. Geophys. Res.*, *103*, 7475–7489, 1998.

Carmack, E. C., K. Aagaard, J. H. Swift, R. W. MacDonald, F. A. McLaughlin, E. P. Jones, R. G. Perkin, J. N. Smith, K. E. Ellis, and L. R. Kilius, Changes in temperature and tracer distributions within the Arctic Ocean: Results from the 1994 Arctic Ocean section, *Deep Sea Res., Part II*, 44, 1487–1502, 1997.

Dickson, R. R., T. J. Osborn, J. W. Hurrell, J. Meincke, J. Blindheim, B. Ådlandsvik, T. Vinje, G. Alekseev, W. Maslowski, and H. Cattle, The Arctic Ocean response to the North Atlantic Oscillation, *J. Clim.*, 13, 2671 ff, 2000.

European Centre for Medium-Range Weather Forecasts (ECMWF), *ECMWF Forecast Model, Physical Parameterization, Res. Manual*, vol. 3, 2nd ed., Reading, U. K., 1988.

Frank, M., Spurenstoffuntersuchungen zur Zirkulation im Eurasischen Becken des Nordpolarmeeres, Ph.D. diss., Ruprecht-Karls-Univ., Heidelberg, Germany, 1996.

Frank, M., W. M. Smethie Jr., and R. Bayer, Investigation of subsurface water flow along the continental margin of the Eurasian Basin using the transient tracers Tritium, ^{3}He, and CFCs, *J. Geophys. Res.*, 103, 30,773–30,792, 1998.

Gerdes, R., Modelling the variability of the exchanges between the Arctic Ocean and the Nordic Seas, in *The Fresh Water Budget of the Arctic Ocean*, edited by E. L. Lewis, pp. 533–547, Kluwer Acad., Norwell, Mass., 2000.

Gerdes, R., and C. Köberle, Numerical simulation of salinity anomaly propagation in the Nordic Seas and the Arctic Ocean, *Polar Res.*, 18, 159–166, 1999.

Gerdes, R., and U. Schauer, Large-scale circulation and water mass distribution in the Arctic Ocean from model results and observations, *J. Geophys. Res.*, 102, 8467–8483, 1997.

Gorshkov, S. G., *Atlas of Oceans: Arctic Ocean*, Mil. Def., Moscow, 1980.

Grotefendt, K., K. Logemann, D. Quadfasel, and S. Ronski, Is the Arctic Ocean warming?, *J. Geophys. Res.*, 103, 27,679–27,687, 1998.

Guay, C. K., and K. K. Falkner, Barium as a tracer of Arctic halocline and river waters, *Deep Sea Res., Part II*, 44, 1543–1569, 1997.

Häkkinen, S., and D. J. Cavalieri, A study of oceanic surface heat fluxes in the Greenland, Norwegian, and Barents Seas, *J. Geophys. Res.*, 94, 6145–6157, 1989.

Häkkinen, S., and G. L. Mellor, Modeling the seasonal variability of a coupled Arctic ice-ocean system, *J. Geophys. Res.*, 97, 20,285–20,304, 1992.

Harms, I. H., and M. J. Karcher, Modelling the seasonal variability of circulation and hydrography in the Kara Sea, *J. Geophys. Res.*, 104, 13,431–13,448, 1999.

Hibler, W. D., III, A dynamic-thermodaynamic sea ice model, *J. Phys. Oceanogr.*, 9, 815–846, 1979.

Holland, D. M., L. A. Mysak, and J. M. Oberhuber, Simulation of the mixed-layer circulation in the Arctic Ocean, *J. Geophys. Res.*, 101, 1111–1128, 1996a.

Holland, D. M., L. A. Mysak, and J. M. Oberhuber, An investigation of the general circulation of the Arctic Ocean using an isopycnal model, *Tellus, Ser. A*, 48, 138–157, 1996b.

Jones, E. P., L. G. Anderson, and J. H. Swift, Distribution of Atlantic and Pacific waters in the upper Arctic Ocean: Implications for circulation, *Geophys. Res. Lett.*, 25, 765–768, 1998.

Karcher, M. J., I. H. Harms, and J. M. Smith, Long-range transport of 129 I and 137 Cs in the Nordic Seas and the Arctic Ocean, paper presented at the International Symposium on Marine Pollution, Int. At. Energy Agency, Vienna, 1999.

Kauker, F., and J. M. Oberhuber, An isopycnical ocean circulation model of the North Sea for dynamical downscaling, *GKSS-Rep. 97/E/47*, GKSS Res. Cent., Geesthacht, Germany, 1997.

Levitus, S., Climatological atlas of the world ocean, *NOAA Prof. Pap. 13*, 173 pp., U.S. Govt. Print. Off., Washington, D. C., 1982.

Maslowski, W., D. C. Marble, W. Walczowski, and A. J. Semtner, On large scale shifts in the Arctic Ocean and sea ice conditions during 1979–1998, *Ann. Glaciol.*, 23, 545–550, 2001.

Mauritzen, C., Production of dense overflow waters feeding the North Atlantic across the Greenland-Scotland Ridge part 1, Evidence for a revised circulation scheme, *Deep Sea Res., Part I*, 43, 769–806, 1996.

McLaughlin, F. A., E. C. Carmack, R .W. Macdonald, and J. K. B. Bishop, Physical and geochemical properties across the Atlantic/Pacific water mass front in the southern Canadian basin, *J. Geophys. Res.*, 101, 1183–1197, 1996.

Oberhuber, J. M., Simulation of the Atlantic Circulation with a coupled sea ice-mixed layer-isopycnal general circulation model, part I, Model description, *J. Phys. Oceanogr.*, 23, 808–829, 1993a.

Oberhuber, J. M., Simulation of the Atlantic circulation with a coupled sea ice-mixed layer-isopycnal general circulation model, part II, Model experiment, *J. Phys. Oceanogr.*, 23, 830–845, 1993b.

Oberhuber, J. M., Description of the parallel isopycnal primitive equation OGCM PIPE, *Tech. Rep. 19*, Dtsch. Klimarechenzentr., Hamburg, 1999.

Östlund, H. G., and G. Hut, Arctic Ocean water mass balance from isotope data, *J. Geophys. Res.*, 89, 6373–6381, 1984.

Pavlov, V. K., and S. L. Pfirman, Hydrographic structure and variability of the Kara Sea: Implications for pollutant distribution, *Deep Sea Res., Part II*, 42, 1995.

Polyakov, I. V., A. Y. Proshutinsky, and M. A. Johnson, Seasonal cycles in two regimes of Arctic climate, *J. Geophys. Res.*, 104, 25,761–25,788, 1999.

Proshutinsky, A. Y., and M. A. Johnson, Two circulation regimes of the wind-driven Arctic Ocean, *J. Geophys. Res.*, 102, 12,493–12,514, 1997.

Quadfasel, D., B. Rudels, and S. Selchow, The Central Bank vortex in the Barents Sea: Watermass transformation and circulation, *ICES Mar. Sci. Symp.*, 195, 40–51, 1993.

Roach, A. T., K. Aagaard, C. H. Pease, S. A. Salo, T. Weingartner, V. Pavlov, and M. Kulakov, Direct measurements of transport and water properties through the Bering Strait, *J. Geophys. Res.*, 100, 18,443–18,457, 1995.

Rudels, B., E. P. Jones, L. G. Anderson, and G. Kattner, On the intermediate depth waters of the Arctic Ocean, in *The Polar Oceans and Their Role in Shaping the Global Environment, Geophys. Monogr. Ser.*, vol. 85, edited by O. M. Johannessen, R. D. Muench, and J. E. Overland, pp. 33–46, AGU, Washington, D. C., 1994.

Rudels, B., L. G. Anderson, and E. P. Jones, Formation and evolution of the surface mixed layer and halocline of the Arctic Ocean, *J. Geophys. Res.*, 101, 8807–8821, 1996.

Schauer, U., R. D. Muench, B. Rudels, and L. Timokhov, Impact of eastern Arctic shelf waters on the Nansen Basin, *J. Geophys. Res.*, 102, 3371–3382, 1996.

Schauer, U., B. Rudels, E. P. Jones, L. G. Anderson, R. D. Muench, G. Björk, J. H. Swift, V. Ivanov, and A.-M. Larsson, Confluence and redistribution of Atlantic Water in the Nansen, Amundsen and Makarov basins, *Ann. Geophys.*, 20, 257–273, 2002.

Schlosser, P., D. Bauch, R. Fairbanks, and G. Bönisch, Arctic river runoff: mean residence time on the shelves and in the halocline, *Deep Sea Res., Part I*, 41, 1053–1068, 1994.

Schlosser, P., J. H. Swift, D. Lewis, and S. L. Pfirman, The role of the large-scale Arctic Ocean circulation in the transport of contaminants, *Deep Sea Res., Part II*, 42, 1341–1367, 1995.

Simonsen, K., and P. M. Haugan, Heat budgets of the Arctic Mediterranean and sea surface heat flux parameterizations for the Nordic Seas, *J. Geophys. Res.*, 101, 6553–6576, 1996.

Smethie, W. M., Jr., P. Schlosser, G. Boenisch, and T. s. Hopkins, Renewal and circulation of intermediate waters in the Canadian Basin, observed on the SCICEX 96 cruise, *J. Geophys. Res.*, 105, 1105–1121, 2000.

Smith, J. N., K. M. Ellis, and T. Boyd, Circulation features in the western Arctic Ocean revealed by nuclear fuel tracers from scientific ice expeditions 1995 and 1996, *J. Geophys. Res.*, 104, 29,663–29,677, 1999.

Swift, J. H., E. P. Jones, K. Aagaard, E. C. Carmack, M. Hingston, R. W. Macdonald, F. A. McLaughlin, and R. G. Perkin, Waters of the Makarov and Canada basins, *Deep Sea Res., Part II*, 44, 1503–1529, 1997.

Trenberth, K. E., J. G. Olson, and W. G. Large, A global ocean wind stress climatology based on ECMWF analyses, *Tech. Note NCAR/TN-338-STR*, Natl. Cent. for Atmos. Res., Boulder, Colo., 1989.

Treshnikov, A. F., *Atlas of the Arktic* (in Russian), 204 pp., Cent. Dir. of Geod. and Cartogr. of the Counc. of Ministers of the USSR, Moscow, 1985.

Vinje, T., N. Nordlund, and A. Kvambekk, Monitoring ice thickness in Fram Strait, *J. Geophys. Res.*, 103, 10,437–10,449, 1998.

Wright, P., An atlas based on the COADS data set: Fields of mean wind, cloudiness and humidity at the surface of the global ocean, *Tech. Rep. 14*, Max-Planck-Inst. für Meteorol., Hamburg, Germany, 1988.

———————

M. J. Karcher, Alfred Wegener Institut für Polar und Meeresforschung, Columbusstrasse, D-27515 Bremerhaven, Germany. (mkarcher@awi-bremerhaven.de)

J. M. Oberhuber, Am Loisachbogen 5a, 82515 Wolfratshausen, Germany. (softspace@t-online.de)